Journal of Advanced Research 12 (2018) 11–19

Contents lists available at ScienceDirect

Journal of Advanced Research

journal homepage: www.elsevier.com/locate/jare

Original Article

Mechanism and rate constant of proline-catalysed asymmetric aldol reaction of acetone and p-nitrobenzaldehyde in solution medium: Density-functional theory computation

Usman I. Tafida [a,b,*], Adamu Uzairu [b], Stephen E. Abechi [b]

[a] Department of Chemistry, Faculty of Science, Abubakar Tafawa Balewa University, Bauchi, PMB: 0248 Bauchi, Bauchi State, Nigeria
[b] Department of Chemistry, Faculty of Science, Ahmadu Bello University, Zaria, PMB: 1044 Zaria, Kaduna State, Nigeria

GRAPHICAL ABSTRACT

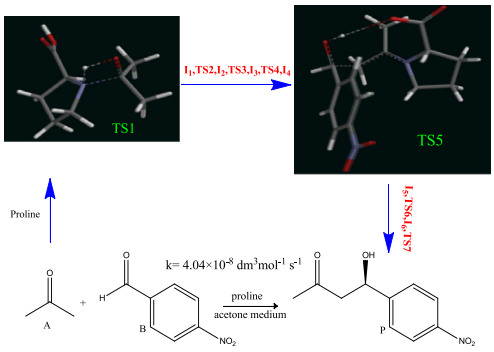

ARTICLE INFO

Article history:
Received 29 December 2017
Revised 1 March 2018
Accepted 3 March 2018
Available online 7 March 2018

Keywords:
HOMO
LUMO
DFT
Proline
Catalyst
Mechanism

ABSTRACT

In search of new ways to improve catalyst design, the current research focused on using quantum mechanical descriptors to investigate the effect of proline as a catalyst for mechanism and rate of asymmetric aldol reaction. A plausible mechanism of reaction between acetone and 4-nitrobenzaldehyde in acetone medium was developed using highest occupied molecular orbital (HOMO) and lowest unoccupied molecular orbital (LUMO) energies calculated via density functional theory (DFT) at the 6-31G*/B3LYP level of theory. New mechanistic steps were proposed and found to follow, with expansion, the previously reported iminium-enamine route of typical class 1 aldolase enzymes. From the elementary steps, the first step which involves a bimolecular collision of acetone and proline was considered as the rate-determining step, having the highest activation energy of 59.07 kJ mol^{-1}. The mechanism was used to develop the rate law from which the overall rate constant was calculated and found to be 4.04×10^{-8} d m^3 mol^{-1} s^{-1}. The new mechanistic insights and the explicit computation of the rate constant further improve the kinetic knowledge of the reaction.

Introduction

Asymmetric aldol reaction is a crucial method for constructing carbon-carbon bonds in an enantioselective fashion. Historically, the aldol reaction was discovered by Charles-Adolphe Wurtz in

Peer review under responsibility of Cairo University.
* Corresponding author.
E-mail address: nuraintafida2005@gmail.com (U.I. Tafida).

https://doi.org/10.1016/j.jare.2018.03.002
2090-1232/

1872 as one of the most powerful transformations in organic chemistry [1]. The process unites two carbonyl partners to give β-hydroxyketones with up to two new stereocenters. The reaction requires two carbonyl compounds which may or may not be the same. One of the carbonyl compounds must contain a C—H group bonded to the carbonyl (C=O) group. The hydrogen is called α-hydrogen [2].

The reaction has significant applications in biochemistry [3]. For example, an aldol condensation reaction occurs in the synthesis of glucose, and the reverse of this reaction occurs in the catabolism of glucose. The breakdown of fructose-1,6-bisphosphate into dihydroxyacetone and glyceraldehyde-3-phosphate in the second stage of glycolysis is an example of a reverse aldol reaction catalysed by the enzyme aldolase A (also known as fructose-1,6-bisphosphate aldolase). More so, in the glyoxylate cycle of plants and some prokaryotes, isocitrate lyase produces glyoxylate and succinate from isocitrate. Following deprotonation of the OH group, isocitrate lyase cleaves isocitrate into the four-carbon succinate and the two-carbon glyoxylate via an aldol cleavage reaction. The mechanism of this cleavage is very similar to that of aldolase A reaction of glycolysis [4].

This study aims at proposing a plausible mechanism for a selected proline-catalysed aldol reaction (Scheme 1), which will be used to develop the rate law and subsequently deduce the rate constant.

Proline was shown to possess catalytic activity as well as enantioselectivity upon asymmetric aldol reaction [5,6] in previous studies, including the pioneering work of Hajos-Parrish-Eder-Sauer-Wiechert [7,8]. It is a viable organocatalyst for several other asymmetric transformations, such as Mannich and Michael additions [9–11]. The mechanism of the reaction, as seen in Scheme 2, was proposed to proceed via iminium-enamine transformation [5] as was discussed by Jung [12] and, later, Hoang et al. [13]. The enantioselectivity- determining step of the mechanism was found to be influenced by proline [14–16]. Blackmond et al. used Reaction Progress Kinetic Analysis (RPKA) to investigate the dependence of

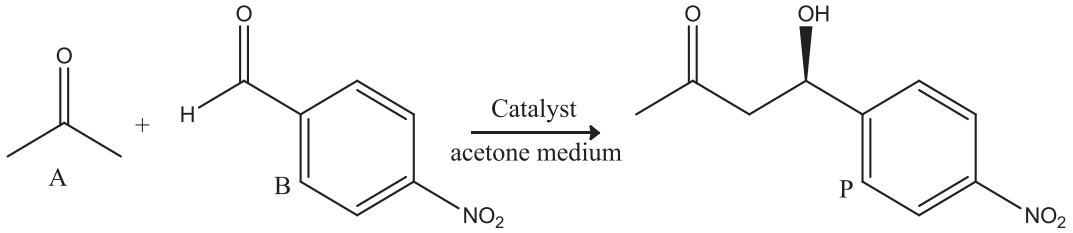

Scheme 1. catalysed aldol reaction between acetone and 4-nitrobenzaldehyde taking place in acetone medium.

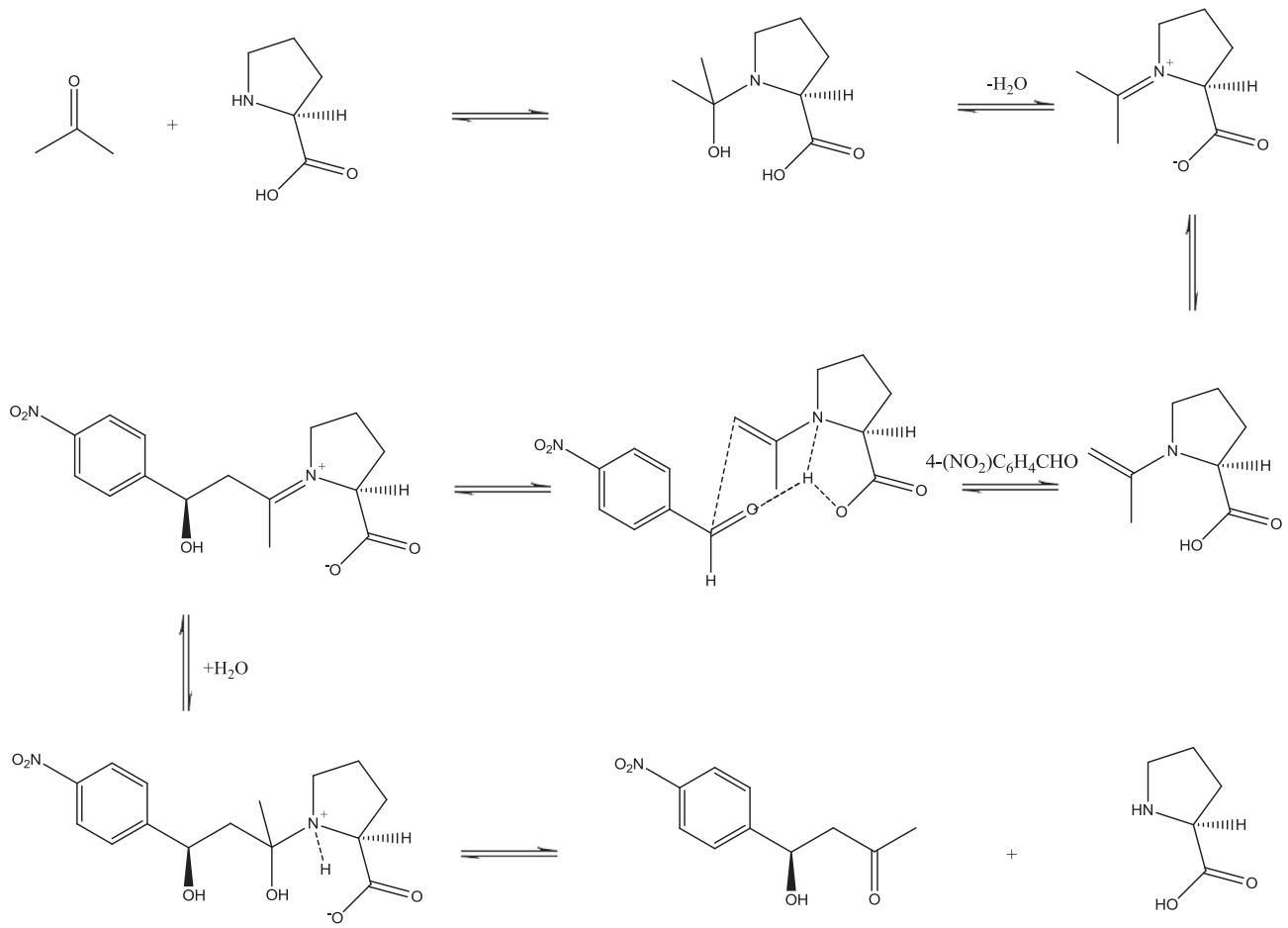

Scheme 2. Reported mechanism of proline-catalysed aldol reaction between acetone and 4-nitrobenzaldehyde.

the reaction rate on the reactants' concentrations and proposed a rate law [17]. More recently in 2016, Ceotto et al. improved upon the rate law, taking into consideration the reversibility of the elementary steps [18]. Previous works indicated that enamine formation and/or carbon-carbon bond formation is the rate-determining step [19–22]. However, the work of Boyd et al., which utilizes the density-functional method in acetone medium, found that the initial complexation between proline and acetone required the highest activation energy [23]. However, there was a significant energy drop upon carrying out the reaction in a different medium (Dimethyl sulfoxide). As such, the step is the rate-limiting but only in acetone medium [23].

Central to the computations in this work is the determination of transition state structures. Unlike stable molecules, the transition state structures do not exist practically. Therefore, they cannot be measured experimentally [24,25]. However, measured activation energies can help to determine the transition state energies relative to reactants. This is informed by the transition state theory which assumes that all reactants pass through a single transition state for every transformation [24]. Like reactants, intermediates, and products, the transition states correspond to structures which can be found and characterized by theoretical calculations almost as routinely as finding equilibrium geometry [25–27]. After finding the transition state geometry, it needs to be tested to confirm that it is the transition route with the minimum energy. The first test requires carrying out Infra-Red (IR) analysis on the proposed transition structure to verify that its Hessian contains only one imaginary frequency in the range of 400–2000 cm^{-1} [28,29]. Secondly, the coordinate corresponding to the imaginary frequency must smoothly connect reactants and products [28,29]. That is, we should be able to walk along this coordinate without any additional optimization. The extent to which transition states incorporate partially broken bonds may prompt anticipating that a simple theoretical model cannot be able to describe the transition state structures effectively. In this regard, Becke-Lee-Yang-Parr 3 Parameters (B3LYP) functional and *polarized* Pople's split-valence double-zeta (6-31G*) basis set perform much better than so many other models [30,31]. However, this model has the disadvantage of consuming very much computer time. It, for instance, takes 72–336 h to compute a single transition state geometry for this reaction, using a Core i5/12 GB RAM personal computer. List's NMR/GC-MS study [32], Houk's Density-Functional Theory (DFT) calculation [33] and several other studies that include both experimental and theoretical works were dedicated on finding new mechanistic insights into proline-catalysed aldolization using different combinations of aldehydes and ketones. However, most of these works relied on guessed transition states [34–36]. In the current study, we tried to adopt a more specific method of using quantum mechanical descriptors of Highest Occupied Molecular Orbital energy (E-HOMO) and Lowest Unoccupied Molecular Orbital energy (E-LUMO) to propose the transition states. This approach minimizes trial and error in identification of mechanistic steps of the reaction. More so, the work links the quantum mechanical parameters to the reaction rate. The rate constant depends on the thermodynamic parameters (enthalpy of activation and entropy of activation) of the elementary steps which can only be deduced after identifying the transition structures. And then, the transition state structures are built based on the HOMO-LUMO gaps of the combining molecules. The significance of this link is that it can provide a logical guide in designing a new catalyst that can facilitate higher reaction rate by looking into the atomic and electronic properties of the candidates for favourable HOMO and LUMO energy values.

Computational details

All the structures of the compounds, transition states, and intermediates involved were built using Wavefunction Spartan 14 V1.1.4 [15] and subjected to energy minimization to remove their strain energies. DFT was adopted in calculating the equilibrium geometry of the compounds and intermediates; and transition state geometry of the transition states using B3LYP functional and 6-31G* basis set as built-in in Spartan 14 software [29,37]. The bond lengths were obtained after optimizing the structures. The energies of HOMO and LUMO as well as the thermodynamic parameters were equally generated from the said calculation and recorded for all the reaction steps.

Solvation Model 8 (SM8) continuum model as built-in in Spartan 14 was adopted to calculate the effect of solvent on the energies and wave functions [29]. An additional calculation, Intrinsic Reaction Coordinate (IRC), was carried out to signify that the resulting transition state can be used to generate a pathway leading first to the reactants and then to the products.

Results and discussion

Mechanism

Fig. 1 presents the two-dimensional potential energy profile of the reaction. This chart is only useful in displaying the energy

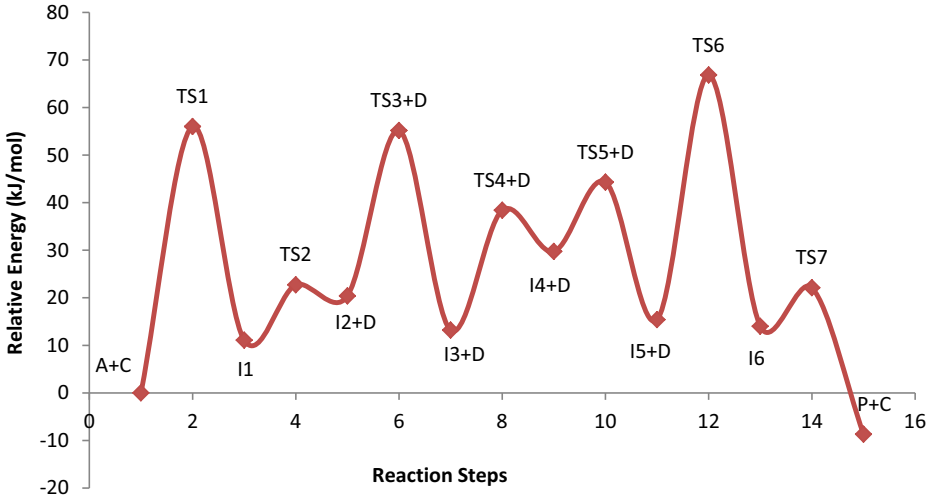

Fig. 1. Energy Barrier Chart for the mechanistic steps of the proline-catalysed reaction of acetone and 4-nitrobenzaldehyde.

Table 1
Results of E-HOMO and E-LUMO computations.

Steps	E-HOMO (eV)	E-LUMO (eV)	HOMO Centre	LUMO Centre
A	−6.56	−0.11	=O	=C
B	−7.18	−2.86	=O···C	=C···O
C	−6.36	0.60	—N—	=C
D	−7.86	1.89	O	H
TS1	−5.44	0.04		
I_1	−5.65	−0.12	—N—	=C
TS2	−6.05	0.37		
I_2	−5.44	−1.07	O^-	=C
TS3	−6.28	−0.76		
I_3	−6.16	0.33	O	H
TS4	−5.63	−0.49		
I_4	−5.07	0.17	=C	H···O
TS5	−5.23	−2.39		
I_5	−5.89	−2.41	=O···C	=C···N
TS6	−9.00	−4.04		
I_6	−5.53	−1.25	O^-	H···O
TS7	−6.21	−1.26		
P	−6.79	−2.40		

barriers of all the reaction steps. The actual enthalpies and Gibb's free energies are available in the Supplementary materials. The y-axis is the relative energy of the system, and the x-axis is the reaction coordinate which corresponds to the geometry of the system at various points. The sum of enthalpies of formation of acetone (A) and proline catalyst (C) forms the energy minimum at 0 kJ mol^{-1}.

From the results of E-HOMO and E-LUMO of all the reaction species given in Table 1, acetone (A) is seen to have the E-HOMO value of −6.56 eV and E-LUMO value of −0.11 eV. The catalyst proline (C) has the E-HOMO and E-LUMO values of −6.36 eV and 0.60 eV, respectively.

According to Molecular Orbital (MO) theory, HOMO and LUMO are the frontier orbitals, which are the most involved MOs in chemical reactions. It is imperative to note that most chemical reactions involve electron transfer between orbitals with HOMO being the donor orbital and LUMO being the acceptor orbital. For a successful interaction, the energy input required for electron movement should be at the minimum. Where more than one set of reagents can combine, there exists a competition as to which combination would react first. Conventionally, we can identify the most favourable combination by examining the energies of the frontier orbitals. It is reasonable to assume that the reagent with the highest energy HOMO will give up its electrons easier and be the most reactive nucleophile, while, the reagent with the lowest energy LUMO will accept electrons most readily, and be the most reactive electrophile. The extent to which MOs combine depends on the degree of overlap (S) and the energy difference between MOs ($\Delta\varepsilon$) in a relation: $S^2/\Delta\varepsilon$. Hence, for a mixture of several combinations of competing nucleophiles and electrophiles, the fastest chemical reaction would be the one that involves the reagent combination of the smallest HOMO-LUMO energy gap ($\Delta\varepsilon$). This means the HOMO and LUMO with narrower energy gap combine more readily than the ones with a wider gap. The narrowest HOMO-LUMO gap in the combination of A and C, as demonstrated in Fig. 2, is between the HOMO of C and LUMO of A.

The LUMO of acetone and the HOMO of proline are given in Fig. 3b and d, respectively. By convention, the blue and red colours show the positive and negative values of the orbital, respectively. The LUMO is delocalized onto several atoms and it is difficult to tell where exactly a pair of electrons (a nucleophile) will attack the molecule. A better portrayal is provided by LUMO-map, which paints the absolute value of LUMO on the electron density surface. By convention, the blue colour represents the highest concentration of the LUMO while the red colour represents the lowest. The

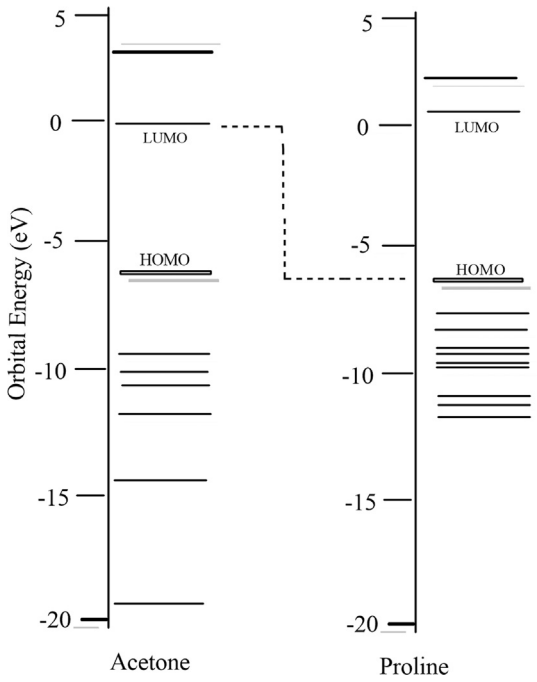

Fig. 2. Identifying the narrowest HOMO-LUMO gap of A versus C.

LUMO-map of acetone is shown in Fig. 3e where the LUMO is seen to concentrate on the carbonyl carbon atom. Although the HOMO delocalizes over several sites, the largest contribution comes from the Nitrogen atom. This finding is supported by Fig. 3g, showing the HOMO-density of proline, which maps the absolute value of HOMO on to the electron density surface. Observing the region with the bluest colouration in the HOMO-density map, we confirm that the HOMO resides more on the Nitrogen atom. Therefore, we expect electron movement and bond formation to occur at that Nitrogen.

Local ionization potential map is used to identify the centres of electrophilic or nucleophilic attack on a molecule. By convention, regions toward red indicate areas from which ionization is relatively easy; therefore, they are subject to electrophilic attack. Regions in blue indicate the areas where ionization is relatively difficult. The carbonyl carbon of acetone, as shown in Fig. 3f displays the highest blue colouration and considered to be the centre for nucleophilic attack. While the nitrogen atom of proline, as shown in Fig. 3h, bears the least blue colour and is considered to be closest to the red colour, hence, taken as the centre for electrophilic attack. More so, the shape of the frontier orbitals is useful as a guide in determining reactivity. In Fig. 4, we can see that the frontier orbitals are poised to undergo a symmetry-allowed interaction in such a way that the positive part of the HOMO interacts with the positive part of the LUMO, also the negative part of the HOMO interact with the negative part of the LUMO, thereby allowing a positive overlap throughout. The two interactions reinforce, and the total frontier orbital interaction is non-zero. Therefore, according to Fukui-Woodward-Hoffmann rules [38,39], electron movement giving rise to the chemical reaction can occur.

The N atom of C, therefore, attacks the carbonyl carbon of A, forming a C···N bond of 1.628 Å, while O of acetone mechanically attacks H atom attached to N of proline, forming an O···HN bond of 1.352 Å. Following such attacks, transition state 1 (TS1) structure (Scheme 3a) forms at 56.6 kJ mol^{-1} above reactants' energy. TS1 was identified by an imaginary frequency of 1633 *Hz*, and an IRC plot which shows a smooth connection between the reactants and the desired product. Fig. 5 presents the IRC plot for the

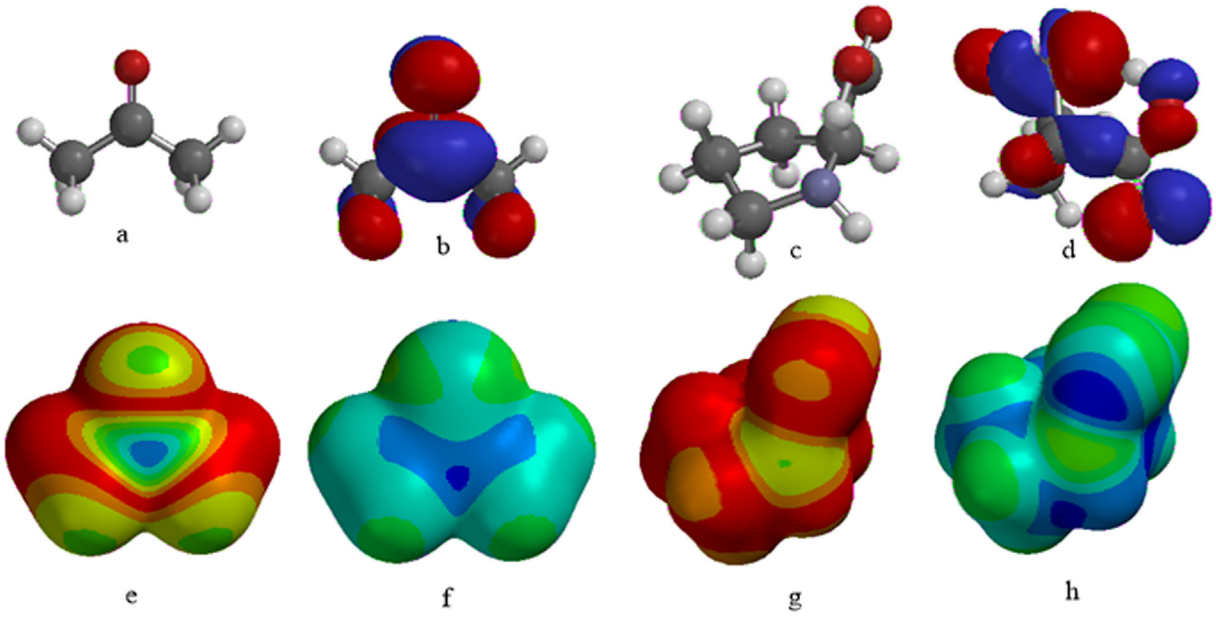

Fig. 3. Potential (a) 3D structure of acetone (b) LUMO of acetone (c) 3D structure of proline (d) HOMO of proline (e) LUMO Map of acetone (f) Local Ionization Potentia map of acetone (g) Density of HOMO of proline (h) Local Ionization Potential of proline.

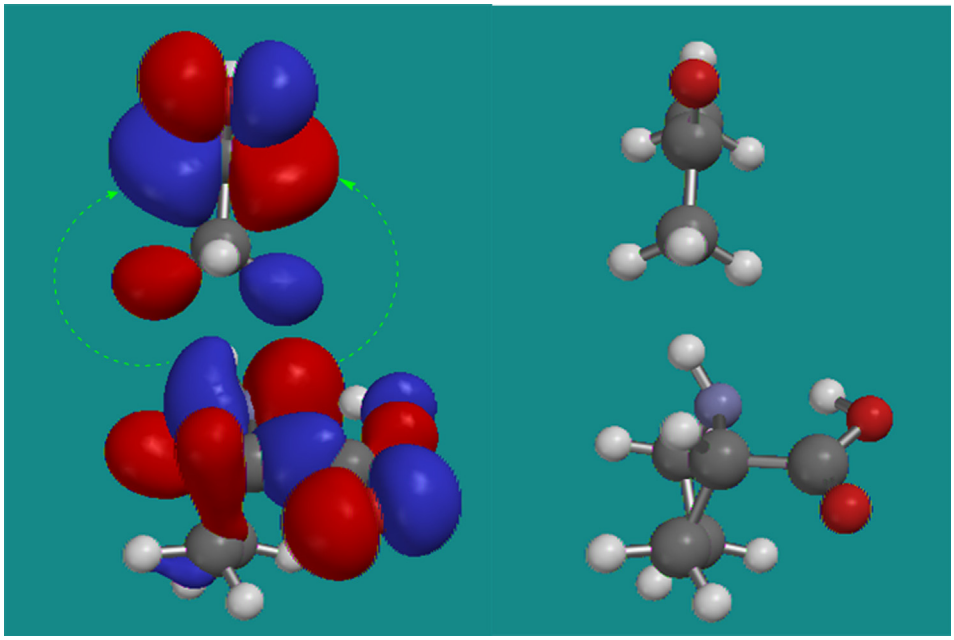

Fig. 4. Symmetry allowed interactions of the HOMO of proline and LUMO of acetone.

formation of TS1, while the plots for the rest of the transition states are available in the supplementary materials.

As C—N bond completely forms at 1.456 Å and N—H bond breaks, an intermediate, I_1 is formed at 11.09 kJ mol^{-1}. Considering all the HOMO-LUMO gaps involved among the species in the reaction setting, viz, A, C, and I_1, the smallest gap is found to be between the HOMO of I_1 (−5.65 eV on N) and its LUMO (−0.12 eV distributed among C= and C). This situation leads to the formation of TS2 at 22.70 kJ mol^{-1} as HO···HO bond of 1.643 Å forms and C···OH bond stretches to 1.495 Å in preparation for removing a water molecule. TS2 was confirmed to be a transition state by an imaginary frequency from IR plot at 1586 Hz and an IRC plot given in supplementary materials. When TS2 finally transforms to iminium ion, I_2; lying slightly below TS2 at 20.39 kJ mol^{-1}, a water molecule (D) is completely removed but remains fused with I_2. With HOMO of −5.44 eV concentrating on O^-, and LUMO of −1.07 eV centering on =C, a C—O bond 3.85 Å long is created within the I_2 to form a transition complex (TS3), fused with D, at 55.16 kJ mol^{-1} above reactants' level. The IR plot of TS3 showed an imaginary frequency of 1999 Hz and the IRC appeared to connect smoothly the I_2 and I_3 via TS3. As C=N π bond breaks and C—O bond contracts to 1.501 Å, TS3 stabilizes to I_3 which, conflated with D, occupies an energy position of 13.2 kJ mol^{-1} above ground level. The I_3, having the E-HUMO of −6.16 eV and E-LUMO of 0.33 eV, would rather rearrange than interact with any other chemical species in the setting. The O atom, therefore, attacks either of the

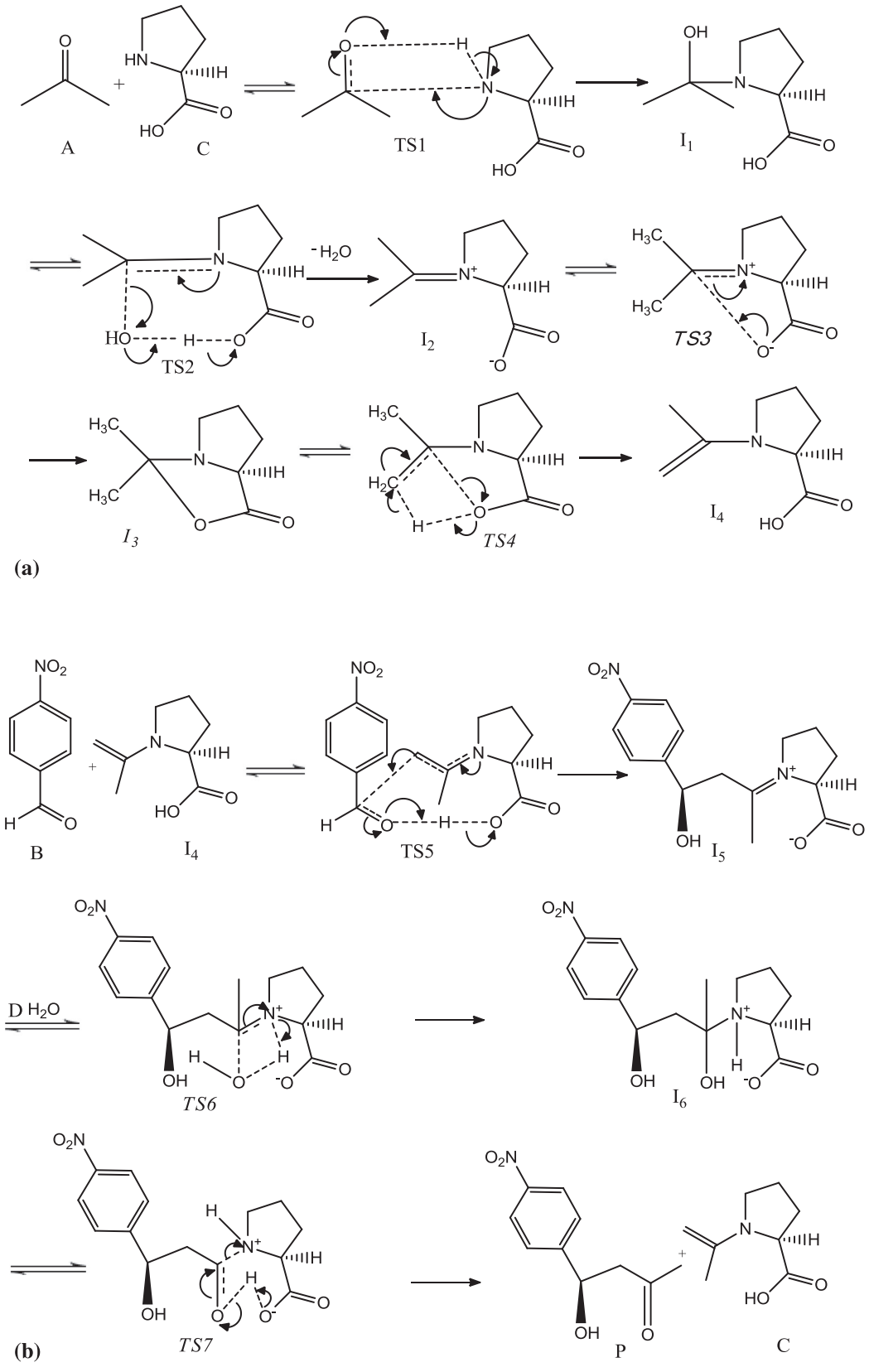

Scheme 3. Proposed mechanism of proline-catalysed aldol reaction of aceton and 4-nitrobenzaldehyde. (3a) Iminium-enamine transformation (3b) C—C bond formation upon addition of 4-nitrobenzaldehyde.

hydrogen atoms of H-CH_2 moieties, forming an O···H bond of 1.24 Å. Mechanically driven breakage of C—H and C—O bonds begins as they stretch to 1.386 Å and 2.982 Å respectively. In the other hand, C—C π bond occurs to complete the transition structure TS4, with the relative energy of 38.4 kJ mol^{-1}, in coalescence with D. Analysis of IR plot confirmed TS4 to be true transition state giving an

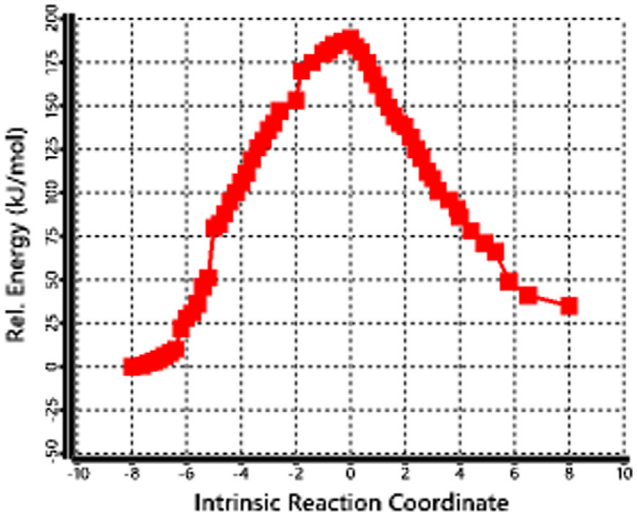

Fig. 5. Plot of TS1 over Intrinsic Reaction Coordinate.

imaginary frequency of 1421 *Hz*. IRC calculation also gave a favourable result for this step. Upon completion of this transition step, enamine (I_4) is formed with a C=C bond of 1.354 Å at 29.76 kJ mol^{-1}, conflated with D. Some previous works assumed a single transition state in iminium-enamine conversion [5,19,20]. However, the supposed transition state (that would have been TS3) was found to have overwhelmingly higher energy barrier (91 kJ mol^{-1}) than the two-step pathway with TS3 (34.77 kJ mol^{-1}) and TS4 (25.2 kJ mol^{-1}) as demonstrated in Fig. 6.

Enamine interacts with nitrobenzaldehyde via a C···C bond of 1.585 Å that occurs between C= of enamine, bearing E-HOMO of −5.07 and =C···O of nitrobenzaldehyde, with E-LUMO of −2.86. Agami et al. have demonstrated that this particular step involves second proline molecule [14]. However, due to careful analysis of HOMO-LUMO gaps involved for the entire species in the reaction setting up to this step, it is found that the interaction with proline molecule with E-HOMO of −6.36 eV is energetically unfavourable. Therefore, the interaction kicks up as aforementioned and proceeds by proton transfer from OH of proline to the carbonyl oxygen of benzaldehyde, via formation of the O···H bond of 0.975 Å and breakage of the other H···O bond by elongating to 2.44 Å. The net structure is the transition complex TS5 (Scheme 3b) of relative energy 44.32 kJ mol^{-1}. An imaginary frequency of 474 *Hz* and a smooth IRC plot shows TS5 to be true transition state. Upon complete proton transfer and contraction of C—C bond to 1.580 Å, a stable intermediate, I_5, forms at 15.41 kJ mol^{-1} above ground level.

The next most favourable interaction is between the HOMO of D, with the energy value of −7.86 eV (on O) and LUMO of I_5 with the energy value of −2.41 eV (on C=···N). An O···C bond of 1.537 Å, therefore, forms between the water molecule and intermediate I_5, and N^+ entraps one H of D and forms a partial N···H bond of 1.450 Å. The resultant transition structure TS6 lies at the energy level of 66.84 kJ mol^{-1}, with an imaginary frequency of 1983 *Hz* and smooth IRC plot, before transforming to I_6 at the energy level of 14.01 kJ mol^{-1} above ground state. The HOMO centre of I_6 is at O^- with the energy value of −5.53 eV while the LUMO centre is at H of OH group at α position to N^+ with the energy value of −1.25 eV. An O···H bond with a bond length of 1.096 Å forms. This bond formation causes H to break from its previous bond with O and allows the O to condense to a carbonyl group. As the C—O double bond forms, the C—N^+ bond stretches to 1.679 Å. The entire process leads to the formation of transition state structure TS7 at 22.12 kJ mol^{-1}, identified by an imaginary frequency of 1275 *Hz* and favourable IRC plot, which splits to give back proline catalyst C and the aldol product, P at 8.68 kJ mol^{-1} lower than the ground level.

Rate constant

Scheme 4 presents the elementary steps. The activation energies were calculated using Eq. (1), which is applicable to both unimolecular and bimolecular solution-phase reactions [37,40].

$$E_a = \Delta H^{\neq} + RT \quad (1)$$

$\Delta H^{\neq}$ is the enthalpy of activation for a given elementary step, while T is the Kelvin temperature and R is the molar gas constant. The equation was applied using the temperature of the reactions (298.15 K) and molar gas constant of 8.314 J K^{-1} mol^{-1}.

For step 1; $\Delta H^{\neq} = H_f(TS1) - [H_f(A) + H_f(C)]$

$\Delta H^{\neq} = 56.6 - 0 = 56.6$ kJ mol^{-1}

And

$E_a = 56.6 + 2.47 = 59.07$ kJ mol^{-1}

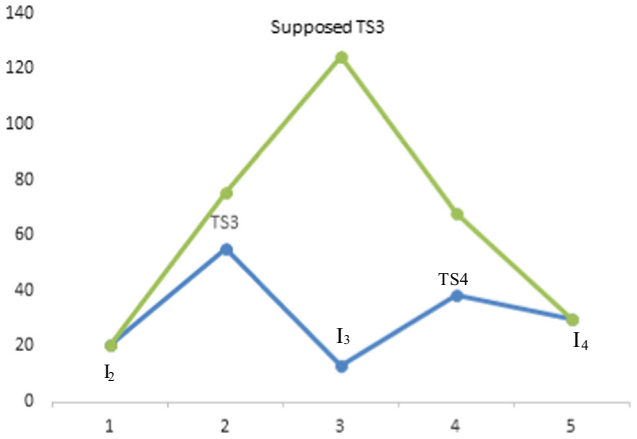

Fig. 6. Comparison between single step and two step mechanism of iminium-enamine transformation.

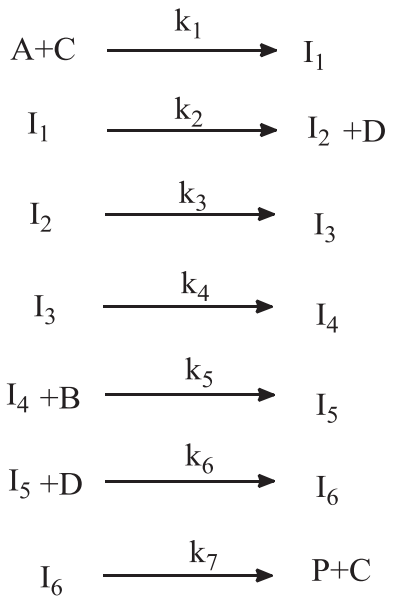

Scheme 4. The elementary steps in the mechanism of proline-catalysed aldol reaction of acetone and 4-nitrobenzaldehyde.

Table 2
Results of enthalpy change, entropy change, activation energies and rate constants calculations.

Elementary steps	$\Delta H^{\neq}$ (kJ mol^{-1})	$\Delta S^{\neq}$ (J mol^{-1} K^{-1})	E_a (kJ mol^{-1})	k [(a) d m^3 mol^{-1} s^{-1} (b) s^{-1}]
A + C → I_1 k_1	56.6	−196.1827	59.07	4.04×10^{-8}a
I_1 → I_2+D k_2	11.63	−2.81	14.10	4.08×10^{10}
I_2 → I_3 k_3	34.77	0.02	37.24	4.82×10^{6}b
I_3 → I_4 k_4	25.20	8.77	27.67	6.62×10^{8}b
I_4+B → I_5 k_5	14.56	−235.83	17.03	8.22×10^{-3}a
I_5+D → I_6 k_6	51.43	−157.53	53.90	3.24×10^{-5}a
I_6 → P + C k_7	8.77	3.51	11.24	2.75×10^{11}b

Even though the elementary steps comprise both endergonic and exergonic processes, the overall reaction is an exergonic reaction with $\Delta H = -8.68$ kJ mol^{-1}. This suggests that the reaction is energetically favourable, having a net gain in energy.

The addition of proline to acetone has the highest activation energy (59.07 kJ mol^{-1}) followed by the step involving the addition of water to C—C complex (53.90 kJ mol^{-1}). We observed a reasonable trend is in the relationship between activation energies and the HOMO-LUMO gaps of the combining MOs, in the sense that the two steps with the highest activation energies happen to have wider HOMO-LUMO gaps (6.25 eV and 5.45 eV, respectively). This trend can be related to the fact that the HOMO with lower energy is comparably more stable and disinclined to release electron for bonding than the HOMO with higher energy. The separation of the HOMO from LUMO corresponds to the amount of energy needed to excite an electron. Therefore, higher activation energy is needed to achieve a reaction in the case of HOMOs at lower energy level further away from LUMOs than in the case of HOMOs at higher energy levels closer to LUMOs.

Having the highest reaction barrier (59.07 kJ mol^{-1}) the rate-determining step (RDS) is, therefore, step 1, and the rate law is as seen in Eq. (2):

$$\frac{d[P]}{dt} = k_1[A][C] \tag{2}$$

where $k_1 = k_{obs.}$

The reaction is first order in A and C, zeroth order in B and D and second order overall.

Table 2 presents the results of the rate constants of the various elementary steps calculated at 298.15 K from the Eyring equation (Eq. (2)), in which $\Delta S^{\neq}$ is the entropy of activation [40,41,42]. The equation is applicable to only solution-phase bimolecular reactions [42].

$$k = e\frac{K_B T}{hc^0} e^{\Delta S^{\neq}/R} e^{-E_a/RT} \tag{3}$$

Since, $k_1 = k_{obs,}$ the overall rate constant (k_{obs}) is taken to be 4.04×10^{-8} d m^3 mol^{-1} s^{-1}.

Conclusions

The study investigated the mechanism of direct aldol reaction between acetone and 4-nitrobenzaldehyde acted upon by proline as a catalyst in acetone medium, via DFT computation. Quantum mechanical descriptors of HOMO and LUMO energies were used to explore various mechanistic steps. Our findings further proved the already proposed iminium-enamine mechanism [5,12,13,43–45]. However, we identified an intermediate (I_3) and many transition states (TS3, TS4, TS6, and TS7) that were not available in the previous works on this subject. The analyses of IR plots, showing one and only imaginary frequency in each case, and IRC calculation of the suggested structures confirmed them as real transition states.

Conflict of interest

The authors have declared no conflict of interest.

Compliance with Ethics Requirements

This article does not contain any studies with human or animal subjects.

Acknowledgement

We thank Abubakar Tafawa Balewa University, Bauchi for financial support to this research.

Appendix A. Supplementary material

Supplementary data associated with this article can be found, in the online version, at https://doi.org/10.1016/j.jare.2018.03.002.

References

[1] Wurtz CA. On an aldehyde alcohol. Bull Soc Chim Paris 1872;17:436–42.
[2] Martínez A, Zumbansen K, Döhring A, Gemmeren M, List B. Improved conditions for the proline-catalyzed aldol reaction of acetone with aliphatic aldehydes. Synlett 2014;25:932–4.
[3] Liu JB, Liu LJ, Dong ZZ, Yang GJ, Leung CH, Ma DL. An aldol reaction-based iridium (III) chemosensor for the visualization of proline in living cells. Sci Rep 2016;6:36509.
[4] Hu H, Juvekar A, Lyssiotis CA, Lien EC, Albeck JG, Oh D, et al. Phosphoinositide 3-kinase regulates glycolysis through mobilization of aldolase from the actin cytoskeleton. Cell 2016;164:433–46.
[5] List B, Lerner RA, Barbas III CF. Proline-catalyzed direct asymmetric aldol reactions. J Am Chem Soc 2000;122:2395–6.
[6] De D, Bhattacharyya A, Bharadwaj PK. Enantioselective aldol reactions in water by a proline-derived cryptand and fixation of CO_2 by its exocyclic Co(II) complex. Inorg Chem 2017;56(18):11443–9.
[7] Hajos ZG, Parrish DRJ. Asymmetric synthesis of bicyclic intermediates of natural product chemistry. Org Chem 1974;39:1615.
[8] Kutzscher C, Nickerl G, Senkovska I, Bon V, Kaskel S. Proline functionalized UiO-67 and UiO-68 type metal-organic frameworks showing reversed diastereoselectivity in aldol addition reactions. Chem Mater 2016;28 (8):2573–80.
[9] Trost BM, Saget T, Hung CI. Direct catalytic asymmetric Mannich reactions for the construction of quaternary carbon stereocenters. Am Chem Soc 2016;138 (11):3659–62.
[10] Klalwani KG, Sudaai A. Proline-catalyzed enantioselective synthesis of 2,3-disubstituted piperidines. Synlett 2016;27:1339–43.
[11] Jin H, Kim ST, Hwang GS, Ryu DH. L-Proline derived bifunctional organocatalysts: enantioselective michael addition of dithiomalonates to trans-β-nitroolefins. J Org Chem 2016;81(8):3263–74.
[12] Jung ME. A review of annulation. Tetrahedron 1976;32:3–31.
[13] Hoang L, Bahmanyar S, Houk KN, List B. Kinetic and stereochemical evidence for the involvement of only one proline molecule in the Transition States of proline-catalyzed intra- and intermolecular aldol reactions. J Am Chem Soc 2003;125(1):16–7.
[14] Agami C, Meynier F, Puchot C, Guilthem J, Pascard C. Tetrahedron 1984;40:1031–8.
[15] Keeri AR, Gualandi A, Mazzanti A, Lewinski J, Cozzi PG. Asymmetric aldol reaction for the synthesis of trans-oxazolines. Chem Eur J 2015;21: 18949–52.

[16] Martínez R, Berbegal L, Guillena G, Ramón DJ. Bio-renewable enantioselective aldol reaction in natural deep eutectic solvents. Green Chem 2016;18:1724.
[17] Zotova N, Broadbelt LJ, Armstrong A, Blackmond DG. Bioorg Med Chem Lett 2009;19:3934.
[18] Orlandi M, Ceotto M, Benaglia M. Kinetics versus thermodynamics in the proline-catalyzed aldol reaction. Chem Sci 2016;7:5421.
[19] Haindl Michael H, Hioe Johnny, Gschwind Ruth M. The proline-enamine formation pathway revisited in DMSO–rate constants determined via NMR. Am Chem Soc 2015; 137 (40): 12835–42.
[20] Perrin CL, Chang KL. The complete mechanism of an aldol condensation. J Org Chem 2016;81(13):5631–5.
[21] Mei J, Mao J, Chen Z, Yuan S, Li H, Yin H, et al. Mechanism and kinetics of 4-hydroxy-2-butanone formation from formaldehyde and acetone under supercritical conditions and in high-temperature liquid phase. Chem Eng Sci 2015;131:213–8.
[22] Ye R, Zhao J, Yuan B, Liu WC, Faucher FF, Chang M, et al. New insights into aldol reactions of methyl isocyanoacetate catalyzed by heterogenized homogeneous catalysts. Nano Lett 2017;17(1):584–9.
[23] Ranklin KN, Gauld JW, Boyd RJ. Density functional study of the proline-catalyzed aldol reaction. J Phys Chem A 2002;106(20):5155–9.
[24] Ges'u GD, Leli'evre T, Peutrecab DL, Nectouxa N. Jump Markov models and transition state theory: the quasi-stationary distribution approach. Faraday Discuss 2016;195:469–95.
[25] Bhoorasingh PL, West RH. Transition state geometry prediction using molecular group contributions. Phys Chem Chem Phys 2015;17:32173.
[26] Jacobson LD, Bochevarov AD, Watson MA, Hughes TF, Rinaldo D, Ehrlich S, et al. Automated transition state search and its application to diverse types of organic reactions. Chem Theory Comput 2017;13:5780–97.
[27] Maa D, Renb H, Maa J. Full-dimensional quantum mechanics calculations for the spectroscopic characterization of the isomerization transition states of HOCO/DOCO systems. Phys Chem Chem Phys 2017;00:1–3.
[28] Maeda S, HarabuchiY, Ono Y, Taketsugu T, Keiji. Intrinsic reaction coordinate: calculation, bifurcation, and automated search. Int J Quant Chem 2015; 115 (5): 258–69.
[29] Spartan' 14 Wavefunction, Inc., Irvine, CA; 2014.
[30] Legler CR, Brown NR, Dunbar RA, Harness MD, Nguyen K, Oyewole O, et al. Scaled quantum mechanical scale factors for vibrational calculations using alternate polarized and augmented basis sets with the B3LYP density functional calculation model. Spectrochim Acta A Mol Biomol Spectrosc 2015;145:15–24.
[31] Zhang Q, Li B, Huang S, Nomura H, Tanaka H, Adachi C. Nature efficient blue organic light-emitting diodes employing thermally activated delayed fluorescence. Photonics 2014;8:326–32.
[32] List B, Hoang L, Martin HJ. New mechanistic studies on the proline-catalyzed aldol reaction. Nat Acad Sci USA 2004;101(16):5839–42.
[33] Bahmayar S, Houk KN. The origin of stereoselectivity in proline-catalyzed intramolecular aldol reactions. J Am Chem Soc 2001;123:12911–2.
[34] Liu B, Wang J, Pang Y, Ge Z, Li R. Unexpected synthesis of 1,3,5-triarly-1,5-diketones from aryl ketones via di-enamine mechanism. Tetrahedron 2014;70:9240–4.
[35] Gisdon FJ, Culka M, Ullmann GM. PyCPR–a python-based implementation of the conjugate peak refinement (CPR) algorithm for finding transition state structures. J Mol Model 2016;22:242.
[36] Bao JL, Meana-Pa~neda R, Truhlar DG. Multi-path variational transition state theory for chiral molecules: the site-dependent kinetics for abstraction of hydrogen from 2-butanol by hydroperoxyl radical, analysis of hydrogen bonding in the transition state, and dramatic temperature dependence of the activation energy. Chem Sci 2015;6:5866.
[37] Lewers EG. Computational chemistry. Peterborough: Springer Nature; 2016. p. 253–8.
[38] Fukui K. Stereospecifity with reference to some cyclic reaction. Tetrahedron Lett 1965;24:2009.
[39] Hoffmann R, Woodward RB. Orbital symmetries and endo-exo relationships in concerted cycloaddition reactions. J Am Chem Soc 1965;87:4388–9.
[40] Puri BR, Sharma LR, Pathania MS. Engineering chemistry. Chandigarh: Vishal publishing Co; 2014. p. 120.
[41] Eyring H. The activated complex and the absolute rate of chemical reactions. Chem Rev 1935;17:65.
[42] Ashley MA, Hirschi JS, Izzo JA, Vetticatt MJ. Isotope effects reveal the mechanism of enamine formation in l-proline-catalyzed α-amination of aldehydes. J Am Chem Soc 2016;138(6):1756–9.
[43] Burés J, Armstrong A, Blackmond DG. Explaining anomalies in enamine catalysis: "downstream species" as a new paradigm for stereocontrol. Acc Chem Res 2016;49(2):214–22.
[44] Sameera WMC, Hatanaka M, Kitanosono T, Kobayashi S, Morokuma K. The mechanism of iron (II)-catalyzed asymmetric mukaiyama aldol reaction in aqueous media: density functional theory and artificial force-induced reaction study. J Am Chem Soc 2015;137(34):11085–94.
[45] Engel T, Reid P. Physical chemistry. New York: Pearson Prentice Hall; 2006. p. 925.